Journal of Hazardous Materials 439 (2022) 129593

Contents lists available at ScienceDirect

Journal of Hazardous Materials

journal homepage: www.elsevier.com/locate/jhazmat

A new source of representative secondary PET nanoplastics. Obtention, characterization, and hazard evaluation

Aliro Villacorta [a,b], Laura Rubio [a,c], Mohamed Alaraby [a,d], Montserrat López-Mesas [e], Victor Fuentes-Cebrian [e], Oscar H. Moriones [f,g], Ricard Marcos [a,*], Alba Hernández [a,*]

[a] Group of Mutagenesis, Department of Genetics and Microbiology, Faculty of Biosciences, Universitat Autònoma de Barcelona, Cerdanyola del Vallès, Barcelona, Spain
[b] Facultad de Recursos Naturales Renovables, Universidad Arturo Prat, Iquique, Chile
[c] Nanobiology Laboratory, Department of Natural and Exact Sciences, Pontificia Universidad Católica Madre y Maestra, PUCMM, Santiago de los Caballeros, Dominican Republic
[d] Zoology Department, Faculty of Sciences, Sohag University, 82524 Sohag, Egypt
[e] GTS-UAB Research Group, Department of Chemistry, Faculty of Science, Universitat Autònoma de Barcelona, 08193 Bellaterra, Cerdanyola del Vallès, Spain
[f] Institut Català de Nanociència i Nanotecnologia (ICN2-UAB-CSIC-BIST), Campus UAB, Bellaterra, 08193 Barcelona, Spain
[g] Universitat Autonòma de Barcelona (UAB), Campus UAB, Bellaterra, 08193 Barcelona, Spain

HIGHLIGHTS

- A proposed method to get PET nanoplastic samples from plastic bottles is presented.
- Completed physicochemical characterization is provided.
- Cell uptake was evaluated following different methods.
- Different hazard effects were determined.
- The method is extrapolated to other plastic and avoids metal contamination.

GRAPHICAL ABSTRACT

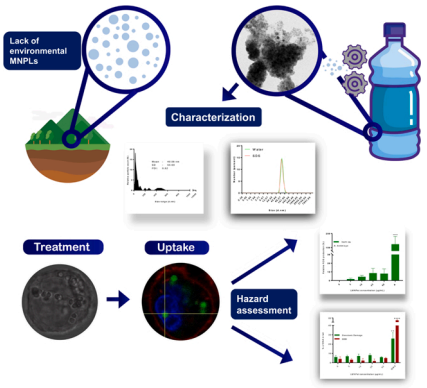

ARTICLE INFO

Editor: Dr. T Meiping

Keywords:
Nanoplastics
Polyethylene terephthalate
Physicochemical characterization
Cell uptake
Cytotoxicity

ABSTRACT

Micro and nanoplastics (MNPLs) are emergent environmental pollutants requiring urgent information on their potential risks to human health. One of the problems associated with the evaluation of their undesirable effects is the lack of *representative samples*, matching those resulting from the environmental degradation of plastic wastes. To such end, we propose an easy method to obtain polyethylene terephthalate nanoplastics from water plastic bottles (PET-NPLs) but, in principle, applicable to any other plastic goods sources. An extensive characterization indicates that the proposed process produces uniform samples of PET-NPLs of around 100 nm, as determined by using AF4 and multi-angle and dynamic light scattering methodologies. An important point to be highlighted is that to avoid the metal contamination resulting from methods using metal blades/burrs for milling, trituration,

* Correspondence to: Group of Mutagenesis, Department of Genetics and Microbiology, Faculty of Biosciences, Universitat Autònoma de Barcelona, Campus of Bellaterra, 08193 Cerdanyola del Vallès, Barcelona, Spain.
E-mail addresses: ricard.marcos@uab.cat (R. Marcos), alba.hernandez@uab.cat (A. Hernández).

https://doi.org/10.1016/j.jhazmat.2022.129593
Received 10 March 2022; Received in revised form 4 July 2022; Accepted 11 July 2022
Available online 14 July 2022

or sanding, we propose to use diamond burrs to produce metal-free samples. To visualize the toxicological profile of the produced PET-NPLs we have evaluated their ability to be internalized by cells, their cytotoxicity, their ability to induce oxidative stress, and induce DNA damage. In this preliminary approach, we have detected their cellular uptake, but without the induction of significant biological effects. Thus, no relevant increases in toxicity, reactive oxygen species (ROS) induction, or DNA damage -as detected with the comet assay- have been observed. The use of *representative* samples, as produced in this study, will generate relevant data in the discussion about the potential health risks associated with MNPLs exposures.

1. Introduction

Despite the multiple advantages of plastic materials, a very dramatic side-effect resulting from this big success is the increased presence of plastic wastes in the environment. Unfortunately, and considering the present capacities of recycling such wastes, this environmental catastrophe will still be increasing and remain for a long (Borrelle et al., 2020).

Once into the environment, plastic wastes degrade due to different abiotic (*i.e.*, photodegradation, physical abrasion, or hydrolysis) and biotic mechanisms (Ali et al., 2021a), generating a new source of contaminants: the micro/nanoplastics (MNPLs). With a size between less than 10 nm and a few mm, MNPLs can be highly mobilized by water and air and, consequently, they can be found in all the environmental niches on a global scale (Evangeliou et al., 2020; Batool et al., 2021). Another characteristic linked to the MNPLs' size is their potential to enter the food web as they can be easily uptaken by living organisms, including humans. In this way, they have become a new group of emergent contaminants with a potential human health risk. In fact, it has been demonstrated that at the nanoscale level MNPLs could exert important biological effects such as reactive oxygen species (ROS) generation, the activation of the immune system by inflammatory responses, and even more, genotoxic DNA damage (Rubio et al., 2020; Ballesteros et al., 2020; Rai et al., 2021).

It should be noted that environmental MNPLs have two different origins. One is associated with the abiotic/biotic degradation of big plastic sizes (macroplastics), as above indicated. In this case, these MNPLs are denominated secondary MNPLs. On the contrary, some MNPLs are synthesized at these small size ranges for specific purposes and are denominated primary MNPLs. One typical example of primary MNPLs is the micro/nanobeads used in exfoliating hand cleansers and facial scrubs. In fact, they are also intentionally added to other many products such as paints, coatings, and inks, or in construction, agriculture/horticulture, and medical products, among others. For these MNPLs, the estimated used amount in Europe is around 145,000 tons per year, and to minimize their impact on the environment and potentially on human health, a restriction on the intentionally-added-microplastic use has been proposed (ECHA, 2018). Regarding the environmental levels of secondary MNPLs they are very difficult to estimate. Nevertheless, it must be remembered that the world production of plastics on 2019 was 368 million tons, that its production is exponentially growing over time, that about 40 % was used for packaging (or single-use), and about 80 % is not properly recycled ending into the environment or landfills (PlasticsEurope 2019; Ali et al., 2021b).

Studies aiming to determine the potential hazard of MNPLs enface big challenges, one being the selection of environmentally representative MNPLs to be used as reference materials. Due to the impossibility of collecting real MNPLs from the environment, especially at the nano range, practically all available studies have used the only MNPLs type that is commercially available in a wide range of sizes, surface modifications, and labeling, which is polystyrene (PS) MNPLs. Hence, all our present knowledge on the potential risk of MNPLs for human health is basically limited to one polymer type. To avoid this bias, some recent alternatives have been proposed aiming at artificially degrade plastic items to obtain new sources of secondary MNPLs to be included in the hazard assessment studies. The pioneering study used the UV-laser ablation process to obtain PET-NPLs (Magrì et al., 2018). Others have used mechanical milling followed by sieve fractionation into MPLs fractions applied to agricultural plastics (a mulch film prepared biodegradable polymer polybutyrate adipate-co-terephthalate and low-density polyethylene (Astner et al., 2019). As well as the trituration of a few millimeters' of industrial PET pellets (Pignattelli et al., 2021). The use of mechanical ground approaches was also proposed to obtain PET-NPLs (Rodríguez-Hernández et al., 2019).

Two important aspects need to be pointed out regarding the so-far proposed alternative protocols to obtain MNPLs. First, polyethylene terephthalate (PET) is used in most of these approaches. This is because, as a thermoplastic polymer, PET do not undergo chemical reactions when heated, and can re-ground several times, what it is very useful for recycling purposes. This, among other reasons, is why PET is one of the major contributors to worldwide plastic wastes (Gwada et al., 2019). Second, many of the proposed methods to obtain degraded MNPLs, such as mechanical milling, allows only to obtain MPLs, but not NPLs. This is very relevant from the toxicological point of view, since it is considered that NPLs have the ability to cross biological primary barriers and, consequently, reach the different organs and tissues after an exposure (Zitouni et al., 2021).

According to the above indicated, it is clear that there is an urgent need to generate new representative MNPLs samples for further use in hazard evaluations (Balakrishnan et al., 2019). In this study, we thoroughly describe our in-house method to obtain PET-NPLs, provide exhaustive characterization of the obtained materials, and assess its usefulness in hazard assessment approaches by analyzing the cellular uptake, cytotoxicity, reactive oxygen (ROS) production, and DNA damage induction in human lymphoblastic cell line models after an acute exposure.

2. Materials and methods

2.1. PET-NPLs obtention

The PET raw material used to produce PET-NPLs was obtained from commercially available water plastic bottles. The developed procedure was adapted from the previously reported by Rodríguez-Hernández et al. (2019). A schematic overview of the used protocol is outlined in Fig. 1. Briefly, pieces of about 12 cm^2 from the bottom part of the water bottles were initially sanded with aluminum oxide/silicon carbide rotary burrs. Due to the observed metal-contamination (as explained in the Results section) a diamond rotary burr sander accessory, attached to a flexible shaft powered by a multitool Dremel 3000, was choose for the sanding process. The obtained PET debris was passed through a 0.20 mm sieve (CISA R-92), and 4 g of the resulting material were dispersed in 40 mL of pre-heated (50 ºC) trifluoroacetic acid (TFA, 90 % v/v), in a proportion of 10 mL TFA per gram of sieved PET, on a stirring plate at 100 rpm for 2 h. After a complete dispersion, the mixture was kept at room temperature overnight in continuous agitation. Next day, 40 mL of TFA 20 % (v/v) was added to the sample and the mixture was kept under constant and vigorous stirring for 24 h. After that, the obtained dispersion was distributed on six 10 mL glass tubes and centrifuged at 2500 RCF for 1 h. Once the supernatants were discarded, the obtained pellets were resuspended on 400 mL of 0.50 % sodium dodecyl sulfate (SDS) solution, vigorously mixed, and distributed into two 200 mL beakers, for

ultrasonication on an SSE-1 Branson sonicator. Sonication lasted for 2 min at 25% amplitude, in 9/9s sonication/break cycles. The volume of each beaker was transferred to a graduated cylinder, where sedimentation of larger particles took place for 1 h. The top 100 mL of the suspension (from each graduated cylinder) was collected and centrifuged as before for SDS elimination, and further washed twice with Mili-Q water and twice with pure ethanol, and let to dry. Pellets were then resuspended on Mili-Q at the desired final concentration, and sonicated at 10 % amplitude for 16 min in a cold-water bath, aliquoted, and immediately frozen on cryotubes in liquid nitrogen and stored at − 80 ºC for further use. Each one of the cryotubes contains 1 mL of a concentration of 12.50 mg/mL.

2.2. Characterization of particle suspension

2.2.1. Scanning electron microscopy/Energy dispersive X-ray microscopy (SEM-EDS)

The stock solution was thawed on a warm bath at 37 °C, and a working solution of 200 μg/mL was prepared on Milli-Q water. A holey carbon grid was dipped into the working solution and water was allowed to evaporate overnight; additionally, a drop was placed on the Si holder. Then, particles in the grid were examined on a SEM Zeiss Merlin (Zeiss, Oberkochen, Germany) coupled with an X-Max 20 mm EDS system (Oxford Instruments, Oxford, UK). In addition to collecting SEM images, for the EDX analysis an area including the nanoparticle surface was selected, and the sample signal was collected and analyzed by the INCA Energy software.

2.2.2. Transmission electron microscopy (TEM)

A working solution of 200 μg/mL was prepared on Milli-Q water and mounted on a holey carbon grid as described above. Particles in the grid were examined by TEM on a JEOL JEM 1400 instrument (JEOL LTD, Tokyo, Japan) operated at 120 kV. TEM imaging was analyzed for particle size distribution using ImageJ software 1.8.0_172 processing and analysis software.

2.2.3. Fourier transform infrared spectroscopy (FTIR)

To detect the functional groups, and to identify the samples as PET, these were analyzed by Fourier-transform infrared spectroscopy (FTIR), as briefly indicated. A drop of particle suspension at a concentration of 1 mg/mL was placed on a gold mirror and let dry for one week inside a petri dish. Analysis was carried out on a Hyperion 2000 microspectrometer using the gold mirror as reference. This analysis was carried out at the Molecular Spectroscopy and Optical Microscopy facility at the *Institut Català de Nanociència i Nanotecnologia* (ICN2). To assess the composition, interferograms were analyzed and contrasted with previous reports.

2.2.4. Multi angle and dynamic light scattering (DLS-MADLS) and zeta potential

The indicative size of the colloid structures in suspension of the hypothetical hard sphere that behave similarly to the particle suspension of the PET-NPLs was analyzed using a Zetasizer® Ultra from Malvern Panalytical. A working solution of 1 mg/mL of PET-NPLs suspension was thawed and then diluted on Milli-Q water for further analysis at a concentration of 200 μg/mL. To investigate better the fraction on the nanoscale, avoiding the masking generated by, agglomerates or particles bigger in size, a sonication for 16 min at 10 % amplitude (as described above), and a filtration step with a 450 μm PES membrane Millex®-HP from Millipore express® was included. To visualize the influence of anionic surfactant as a dispersant of the sample the same procedure described was carried out maintaining the SDS 0.5 % v/v original concentration. Once prepared, the samples were placed on DTS1070 cuvette for surface charge determination by zeta potential measurements, for both water and SDS 0.5 % dispersant. DLS, MADLS and particle concentration measurement were carried out by placing 1.5 mL of the prepared solutions on DTS0012 cuvettes.

2.2.5. Asymmetric flow field flow fractionation (AF4)

The PET nanoparticles separation was performed using the AF2000 Asymmetric Flow FFF system from Postnova Analytics GmbH (Landsberg, Germany) with two PN1130 Isocratic Pumps, a Kloehn V6 Pump, a PN5300 Autosampler, a PEEK AF4 Channel with a 10 kDa regenerated cellulose membrane and a 350 μm height spacer. The mobile phase and the PET suspension were prepared in NovaChem Surfactant 100 (IESMAT, Madrid, Spain) at 0.20 % (v/v). The size data (gyration radius, Rg) was obtained using a PN3609 MALS Detector (9 angles), calibrated with a 125 nm NIST Polystyrene Latex standard (Postnova Analytics GmbH),

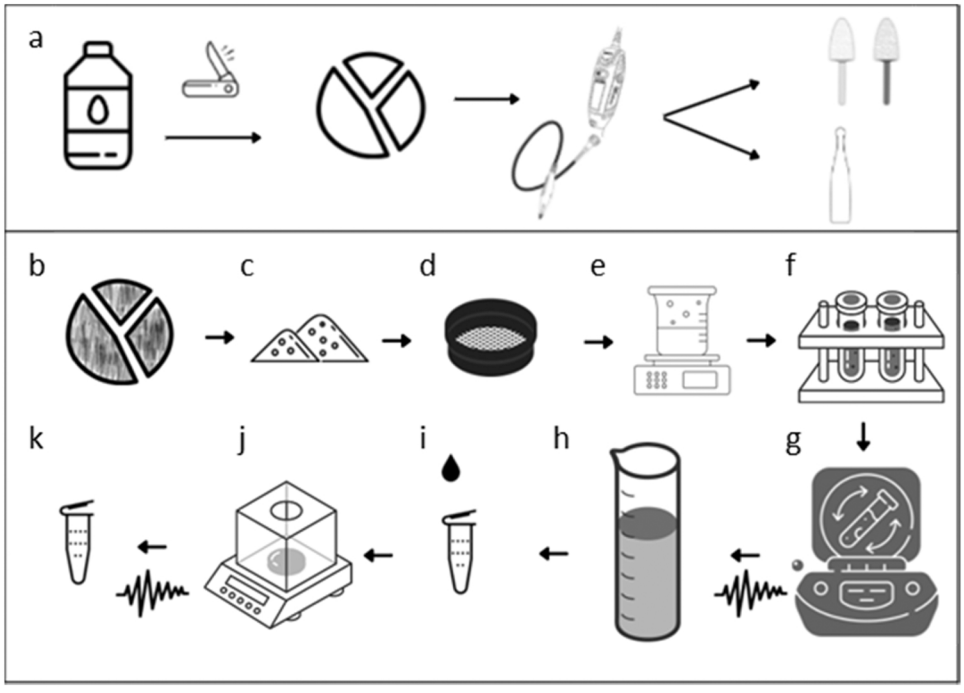

Fig. 1. Schematic representation of the fragmentation and grind process with the mixed burrs or the diamond covered burr (a). Representation of the fractioned pieces (b), PET powder obtained (c) that will be passed through the sieve (d), stirred, suspended, and heated at different concentrations of TFA (e), distributed on glass tubes (f) and centrifuged (g), washed and then resuspended on SDS, sonicated, and transferred to a cylinder for sedimentation (h) and then collected, washed (i), weighted (j), resuspended, sonicated and stored frozen until needed (k).

using the software AF2000 Software and used to calculate the geometric diameter (Dgeo) by dividing 2*Rg by the typical form factor of a sphere (0.78) (Lohrke et al., 2008). The method consisted in three steps, used a constant detector flow of 0.50 mL/min and injections of 20 μL of samples of 1 mg/mL of PET-NPLs suspended in NovaChem 0.20 % were performed. The first step was a focusing step of 3 min with an injection flow of 0.20 mL/min, a cross-flow of 2.00 mL/min and a focus flow of 2.30 mL/min, the second was a separation step, with focus-flow of 0 mL/min, cross-flow from 2.00 mL/min exponential to 0.10 mL/min in 40 min and a final step at a constant flow of 0.10 mL/min of cross-flow during 20 min

2.3. Cell culture

Two human lymphoblastic cell lines were used to detect the potential biological effects of the obtained PET-NPLs, the THP-1 (monocytes) and the TK6 (lymphoblasts). Both cell lines were obtained from Sigma Aldrich (MO, USA) and grown in T-25 flasks containing Roswell Park Memorial Institute (RPMI) medium (Biowest, France) supplemented with 10 % fetal bovine serum (FBS), 1% glutamine (Biowest, France), and 2.5 μg/mL of Plasmocin™ (InvivoGen, CA, USA). Cultures, with a density ranging from 5×10^5 and 1×10^6 cells were maintained at 37 ºC in a humidified atmosphere of 5 % CO_2.

2.4. Cell uptake determination

To confirm the cell uptake of the obtained PET-NPLs, three different approaches have been used: flow cytometry (internal complexity), TEM (internalization), and confocal microscopy (Nile red staining).

2.4.1. Internal complexity

As an indicator of structural complexity of THP1 cells, once the PET-NPLs uptake takes place the orthogonal light scattering -commonly known as Side Scatter (SSC)- was evaluated at concentrations ranging from 0 to 50 μg/mL after exposures lasting for 3 h. The highest concentration (50 μg/mL) was tested in different scenarios in which PET-NPLs were added directly after being rapidly thawed from − 80 ºC on a 37 ºC water bath, then vortexed and resuspended on RPMI media with or without FBS, vortexed again and applied directly to the culture and compared with regular culture conditions with and without FBS. Cells were analyzed by flow cytometry on a CytoFlex s and CytExpert software was used to properly collect means from 10,000 events on the live cell population. Data were analyzed using GraphPad Prism 7.0.

2.4.2. TEM analysis

Exposed cells were fixed in 2 % (w/v) paraformaldehyde and 2.5 % (v/v) glutaraldehyde (Merck, Darmstadt, Germany) in 0.10 M cacodylate buffer (Sigma-Aldrich, Steinheim, Germany) at pH 7.4. After that, cells were processed as already published (Rubio et al., 2016). Briefly, samples were post-fixed with osmium, dehydrated in ethanol, embedded in Epon, polymerized at 60 ºC, and cut with an ultramicrotome. Finally, ultrathin sections placed in copper grids, were contrasted with conventional uranyl acetate and Reynolds's lead citrate solutions and observed using a Jeol 1400 (Jeol LTD) transmission electron microscope equipped with a CCD GATAN ES1000 W Erlangshen camera.

Nile Red stained particles and confocal visualization. Nile red staining of PET-NPLs was carried out following the procedure described in Rodríguez-Hernández et al. (2019) with some important modifications. Briefly, an aliquot (1 mg/mL) was centrifuged for 25 min at 16100 RCF. The supernatant was removed, and 1 mL of Nile red solution (0.50 % in DMSO) was added to the PET-NPLs pellet. The mixture was stirred at room temperature for 24 h (protected from light) at 200 rpm. Successive washes, at least twelve times, with ethanol in 0.10 M PBS, pH 7.40 and resuspended on RPMI supplemented media, prior to cell exposure. For confocal visualization, nuclei were stained using Hoechst 33342 (excitation of 405 nm and emission collected at 415–503), cell membranes were dyed using Cellmask (excitation of 633 nm and emission collected at 645–786). For PET-NPLs labeled with Nile red, an excitation wavelength of 514 nm and emission collected at 546–628 was used. Images of each sample were obtained using a Leica TCS SP5 confocal microscope and processed using ImageJ processing and analysis software. version 1.8.0_172.

2.5. Cell viability assay

Cell viability after exposure to PET-NPLs, was determined using the Beckman counter method. To proceed, cells were seeded at a cell density of 5×10^5 cells/mL on 96 well plates and exposed to a range of concentrations from 0 up to 200 μg/mL of PET-NPLs (200 μg/mL per well). After the exposure time, cells were mixed and diluted 1:100 in ISOFLOW and counted with a ZTM series coulter-counter (Beckman Coulter Inc., CA, USA). The average number of cells counted in each treatment was compared with the average number of the untreated control cells. The results from the viability assay permit to determine the non-cytotoxic concentrations to be used in further experiments.

2.6. Reactive oxygen species (ROS) quantification

Due to the combined capacity of passively diffuse into the cell and being highly reactive, the reduced form of ethidium bromide (dihydroethidium, DHE) was used to detect cytosolic superoxide. Cellular suspensions were seeded on 96 U-type well plates at a cell density of 5×10^5 and treated with concentrations of 5, 10, 25, and 50 μg/mL of PET-NPLs for 3 and 24 h. After the exposure, cells were centrifuged at 1000 rpm for 5 min, resuspended on 10 μM DHE diluted on PBS 1X, to a final cell density of 1×10^6, and incubated for 30 min at 37 ºC. Cells were kept on ice for immediate analysis by using a flow cytometer (Beckman Coulter CytoFLEX S). A total number of 20000 events (single cells) were scored and evaluated using the CytExpert software.

2.7. DNA damage detection: The comet assay

The levels of DNA damage (DNA breaks) in both selected cell lines were evaluated using the published protocol (García-Rodríguez et al., 2019). Both, the overall DNA damage, and the oxidized DNA base levels were determined with the absence/presence of formamidopyrimidine DNA glycosylase (FPG) enzyme. This enzyme detects oxidized DNA bases, excise them, and generate a transient single-strand DNA break detected by the comet assay and denominated as specific oxidative DNA damage (ODD). THP1 cells were exposed to concentrations of 5, 10, 25, and 50 μg/mL of PET-NPLs for 3 h. Treated cells were centrifuged at 0.30 RCF for 8 min at 4 ºC. The obtained pellet was washed and resuspended on cold PBS 1x to get 10^6 cell density per mL. Cells were mixed 1:10 with 0.75 % low melting point agarose at 37 ºC and dropped on triplicates onto GelBond® films (GBFs) (Life Sciences, Lithuania). GBFs containing the samples were treated overnight on cold lysis buffer at 4 ºC and washed on successive 5 and 50 min of enzyme buffer immersion, immediately followed by 30 min incubation at 37 ºC with FPG for the detection of ODD, or without FPG for the detection of general genotoxic damage. GBFs were subjected to electrophoresis (20 V, 300 mA, 4;ºC), washed twice with cold PBS 1X, fixed in absolute ethanol, and air-dried overnight at room temperature. After staining with SYBR Gold, GBFs were visualized in an epifluorescent microscope (Olympus BX50, Hamburg, Germany). The levels of DNA damage, as percentage of DNA in the tail, was quantified with the Komet 5.5 Image analysis system (Kinetic Imaging Ltd, Liverpool, UK). A total of 100 comet images randomly selected were analyzed per sample.

3. Results and discussion

3.1. Characterization of the obtained PET-NPL samples

3.1.1. Morphology and composition

To identify size, shape, and composition of the obtained PET-NPLs, SEM-EDS was used. In Figs. 2a and 2b (as well as in Fig. S1) SEM morphology of the obtained PET-NPLs is visualized. Surface irregularities of the produced particles can be easily observed on the cooper and on the carbon sections of the holder. Not only the differences in size are noticeable, but also the holey structures that can be appreciated. This means that not only the particles are on the nanoscale, but also their surface/volume ratios are different than in a solid body. Interestingly, when energy dispersive X-ray microscopy was used, metal contamination resulting from the sanded process was detected. Thus, in the samples obtained using aluminum oxide/silicon carbide rotary burrs such elements were detected. This metal contamination was not present when a diamond rotary burr was used. This can be observed on Figs. 2c and 2d, and it is summarized on the included table (Fig. 2e). These findings raise an important alarm regarding the abrasive methods to be used in the case of mechanically produced MNPLs, mostly when the potential hazard of the obtained MNPLs need to be evaluated. Surprisingly, this potential metal contamination of the obtained samples is not taken into consideration in neither of the recent published papers using mechanical milling or the trituration of few millimeters' industrial pellets (Astner et al., 2019; Parolini et al., 2020; Lionetto et al., 2021; Pignattelli et al., 2021). The contamination by metals, as consequence of the mechanical milling of other polymers pellets, has also been detected by us, as indicated in Fig. S2, where the results of milling polylactic acid plastic' pellets are indicated. Therefore, from this point forward all the results presented in this study corresponds to the PET-NPLs produced with the diamond burr rotating tool.

From our data, a warning signal must be put to all the hazard data generated using MNPLs obtained using milling procedures, due to the potential metal associated contamination. It is well-know the toxic effects of metals, including those included during the manufacture of plastics (Turner and Filella, 2021).

3.1.2. Dry state size distribution and shape

The TEM images of PET-NPLs reveal a polydisperse anisodiametric particles population with notorious lack of shape regularity. The Martin diameter was measured, and the relative percentage of particle size is represented in Fig. 3a using GraphPad Prism 7.0. The obtained average size of 40.08 nm presents a standard deviation of 55.68 nm and a polydispersity index of 0.52 evidencing the heterogeneity of the PET particles on the suspension produced by this method. Interestingly, the graphic shows a bimodal distribution with a big peak around 50 mm and a second small peak around 500 nm. As an overall, this means that our protocol produces PET particles inside the nano range.

Although the term MNPLs is increasingly used, no general agreement exists on the borders between microplastic and nanoplastic sizes. Engineered nanomaterials are classically considered to range between 1 and 100 nm, but this strict definition leaves out other sizes placed in the nano range. Although engineered materials are built at the desired size, secondary MNPLs are constituted by a wide range of sizes and shapes and some agreement is necessary to define the borders between MPLs and NPLs. At present, many authors consider that MNPLs range from few nm to several mm. To clarify the boundaries criteria, Hartmann et al. (2019) proposed to categorize MNPLs according to the conventional units of size: nano (1–1000 nm) and micro (1–1000 μm). Nevertheless, to maintain the classical definition of nanomaterial/nanoplastic, they proposed to divide the nano range (1–1000 nm) between nanoplastics (1–100 nm) and submicron-plastics (100–1000 nm). Such classification needs to have the general agreement, mostly from those coming from the nanomaterials field. A close inspection of our TEM figures confirms the heterogenicity of the obtained material, which can be considered a realistic characteristic, thereby making it more representative from the environmental point of view. Thus, in addition of the small PET particles of around 50 nm (Fig. 3b), bigger sizes are also present, including rigid fibers (Figs. 3c, 3d), different large shapes (Fig. 3e), and agglomerates (Fig. 3f). Interestingly in Fig. 3f, it is evident that a high amount of PET in the nano range is contained in the agglomerates; nevertheless, the potential biological effects discussed further in this section do not seem to be highly affected by the presence of such agglomerates.

3.1.3. Chemical composition

To confirm the chemical identity of the obtained PET-NPL samples,

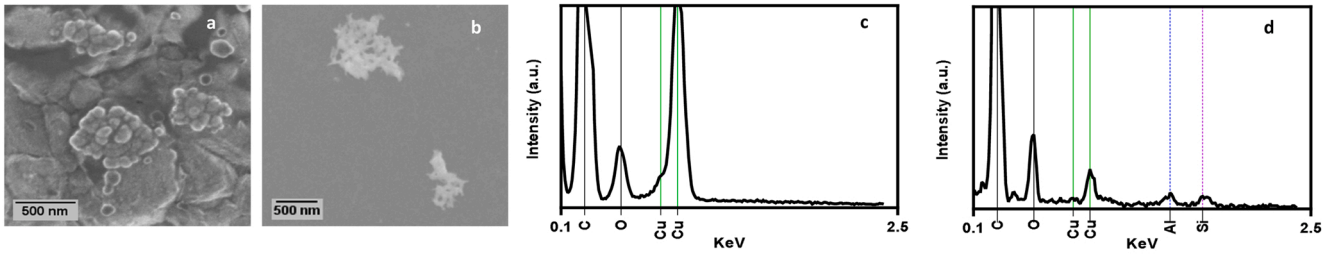

e

	Element							
	C		O		Al		Si	
	Weight (%)	Atomic (%)	Weight (%)	Atomic (%)	Weight (%)	Atomic (%)	Weight (%)	Atomic (%)
LMNPET*	76.68±8.25	87.12±4.63	9.95±2.75	8.59±2.68	3.22±3.48	1.68±1.85	1.45±0.80	0.71±0.40
LMNPET	81.32±6.72	87.84±3.80	13.56±3.13	11.09±3.01	ND	ND	ND	ND

*Produced with aluminum oxide and silicon carbide burrs.

Fig. 2. Scanning electron microscopy results. Amorphous particle structures from a diverse range of geometry can be observed as aggregates metallic section of the holder (a) as in the polymer, where differences in sizes and shapes as well as holey structures can also be detected (b). Notorious differences on the EDS spectra are noticed according to the type of rotating burr utilized where only the diamond covered (c) was able to produce not contaminated samples (d). Aluminum contamination is marked on blue and silica on violet dashed lines, while copper signal marked with green solid lines corresponds to background signal produced by the cooper grid holder. Summary of EDS for both conditions on the table at the bottom (e).

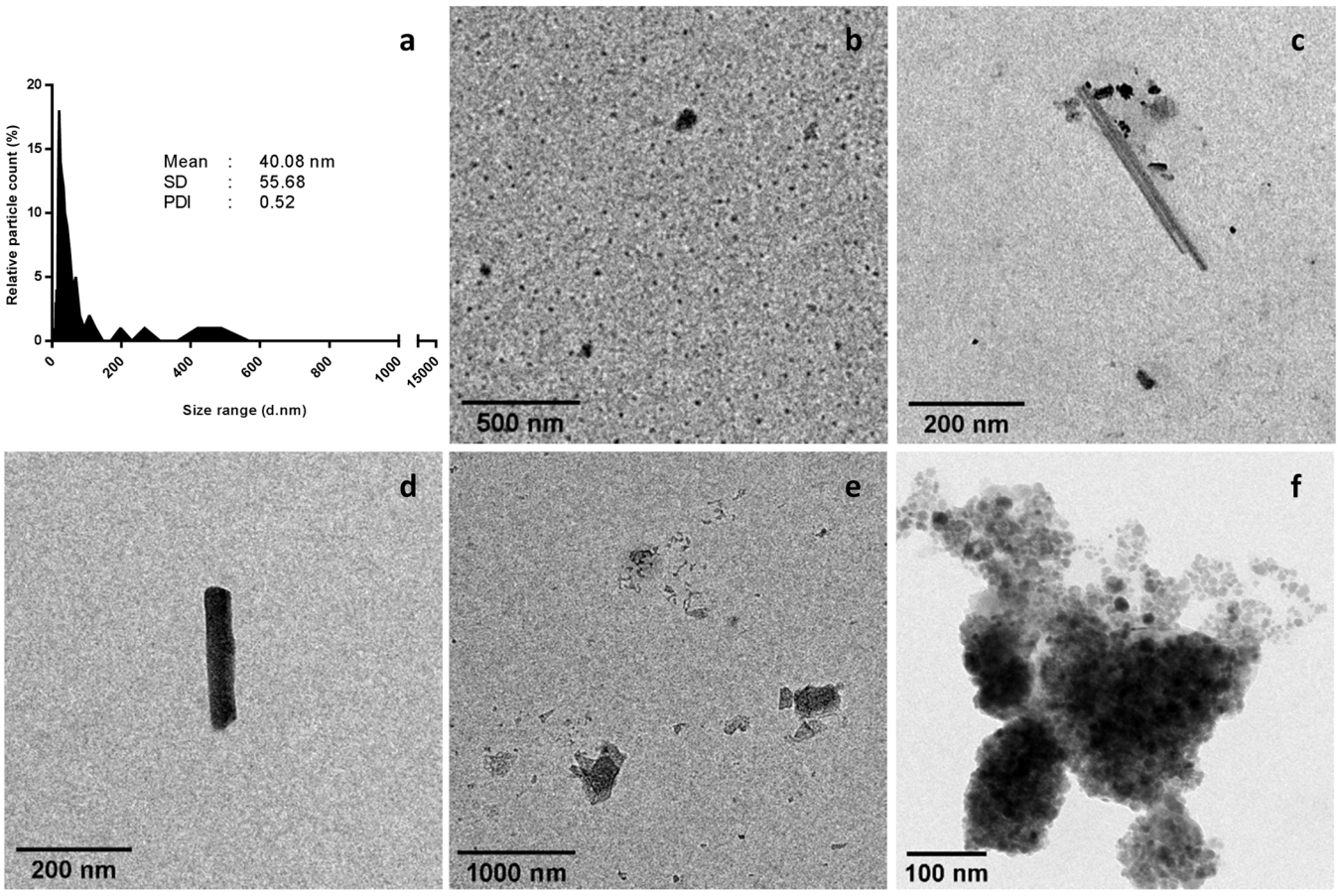

Fig. 3. PET-NPLs characterized by TEM. Size distribution of sizes was obtained from measures of more than 100 images showing a bimodal distribution, with the main peak with sizes around 50 nm, and a second peak with sizes around 400–500 nm (a). Fields with many small sized materials are observed (b), as well as some irregular shapes and fibers (c-e). Agglomerates permit to visualize the small sizes of their components (f).

FTIR analysis was carried out at the premises of the ICN2. To assess the composition of our samples the obtained interferograms were analyzed and contrasted with previous reports of the representative bands present on PET spectrum (Andanson and Kazarian, 2008; Chen et al., 2013; Johnson et al., 2021), and then assigned as reported on Fig. 4. As observed, the obtained peaks match well with the expected, confirming

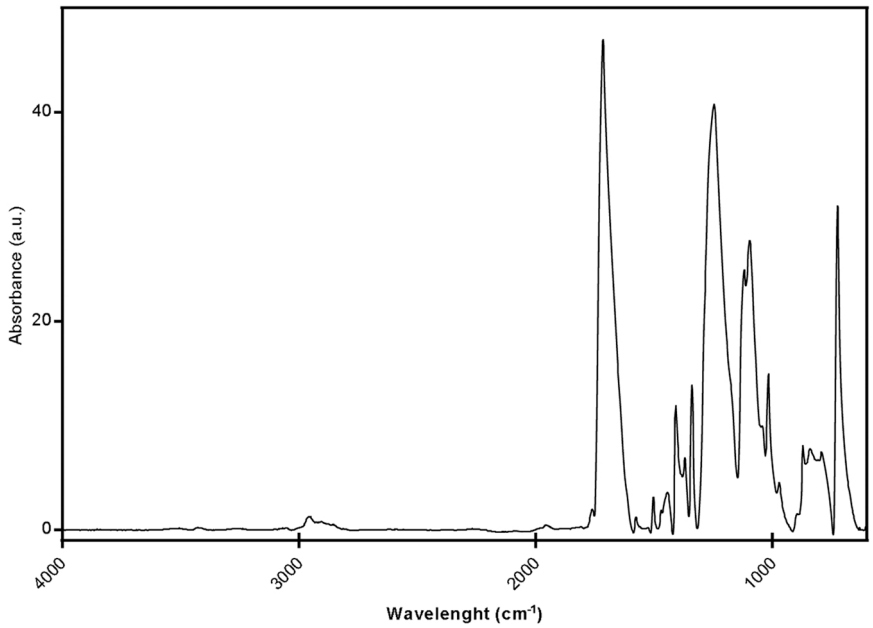

Fig. 4. FTIR spectra with the identity of principal peaks of the interferogram (a) and its assignment (b). Vertical lines indicate coincident peaks.

the PET nature of our samples.

3.1.4. Aqueous solution size distribution and zeta potential

From the bimodal distribution observable by TEM, we tried to reduce the content of the higher-size peak (including agglomerates) by using sonication and/or filtration. This approach is schematized on the Supplementary Fig. S3. According to such approaches, we have observed that the best way to reduce agglomerates includes filtration and sonication. Thus, the characterization of such filtered/sonicated samples by a Zetasizer device is indicated in this section. Other combinations of filtration/sonication and dispersion procedures (Nanogenotox, 2011) are included in Fig. S3. Hydrodynamic diameter measurements by using dynamic light scattering shows mild differences in the average size (of around 30 nm) between the suspension of nanoparticles in water, or with the addition of SDS. The obtained diameter (161.01 ± 3.94 nm) and polydispersity index (PI, 0.22) for aqueous dispersions, slightly differ from those observed using SDS, 129.01 ± 0.94 nm and 0.21, respectively. The corresponding signals, expressed as the mean of three independent measurements, are depicted in Fig. 5a. The correlograms for each condition by triplicates are observed in Fig. 5b. It is interesting to notice that for the mentioned measurements a fixed scattered collection angle of 174.7° was employed, but when the combination of three angles (174.7°, 90°, and 12.78°) are used, the differences or influence of the dispersion media is less noticeable. This can be observed on Fig. 5c, where the curves for both conditions, are almost overlapping. Thus, DLS and even better MADLS are excellent tools for the initial characterization of the obtained PET-NPLs. Another important approach to describe the relative behavior of the particles in suspension is the zeta potential (ZP), which indicates the charge on the surface of the PET-NPLs and the stability of the colloid dispersion. In both cases, summarized on the table (Fig. 5d), the obtained ZP values can be considered as indicative of moderately stable to highly stable suspensions. It is important to remark the important influence of the sample sonication, prior to the characterization, as can be observed in the Supplementary material (Figs. S3 and S4). It is also remarkable that it is possible to calculate the number of particles from the intensity values (Fig. 5d). The obtained values indicate that the used protocol permits to obtain highly concentrated samples.

From the results obtained by the analysis of PET by AF4-MALS, after the void peak at 5 min, a large peak appeared, from min 10–35 with an increase of gyration radius from 30 nm up to 600 nm (Fig. 6a). The 90 % of PET size ranged from 40 nm up to 75 nm of gyration radius (103 up to 194 nm of Dgeo), being 5 % from 75 nm to 100 nm and the rest of the sample above 100 nm (Dgeo above 258 nm), as it can be seen in the Cumulative tendency in Fig. 6b. Moreover, the differential distribution of the PET size, in Fig. 6b, indicated the highest number of particles at approximately 60 nm (155 nm of Dgeo), obtaining a weighted Dgeo of 145 ± 7 nm.

3.2. Cell uptake of PET-NPLs

To demonstrate the potential applicability of the obtained PET-NPLs, as a representative MNPLs material, it is important to find out whether it can be uptake by the cells after having applied a PET-NPLs dispersion and treatment protocol. Herein we have used three different approaches to confirm the cellular uptake in TK6 and THP1 cell models.

3.2.1. Internalization of PET-NPLs stained by Nile red by confocal microscopy

Nanoplastics, in opposition to metallic nanoparticles, are difficult to be visualized by confocal microscopy due to their lack of reflection. Hence, a staining is needed to explore its toxicokinetic behavior by imaging techniques. Among the different staining dyes available that can be applied to plastic particles after its synthesis/obtention, stand up the Nile red. It produced the best results when applied to virgin and weathered synthetic polymers and textile fibers, in comparison with other seven dyes (Prata et al., 2019). In fact, a recent review points out the main pros and cons of the use of the staining dye in the MNPLs context (Shruti et al., 2022) In our case, Nile red staining allowed us to visualize the internalized PET-NPLs inside cells. Due to its affinity for lipidic structures, Nile red signal could induce errors. Nevertheless, we have detected fluorescent signal into the nucleus (Fig. 7a-c) where not structures exist, confirming the usefulness of this staining. Furthers intracellular signals are indicated in Fig. 7g-j, confirming the cell uptake. In fact, the use of Nile red staining was previously found to be useful to detect the cell uptake of other sources of in-house produced PET-NPLs (Rodríguez-Hernández et al., 2019).

3.2.2. Cell complexity as detected by flow cytometry

The first approach was an indirect one checking for structural cell changes due to PET-NPLs exposure. It is expected that cells internalizing PET-NPLs experience changes on their internal structures increasing their granularity, which can be assessed using flow cytometry. As cell granularity increase, an increment of side scattered light is expected, and this effect commonly known as cell-complexity can be observed on Fig. 7e,f. This methodology has shown to be useful in detection cell uptake of different nanomaterials (Vila et al., 2017). From our results, we show that cell uptake is modulated by two factors, such as the exposure time and the presence/absence of FBS. As observed on Fig. 7b, cell uptake increases with the exposure time showing higher uptake after exposures lasting for 3 h regarding the observed after 1 h exposure. In addition, PET-NPLs dispersed in culture media with or without FBS

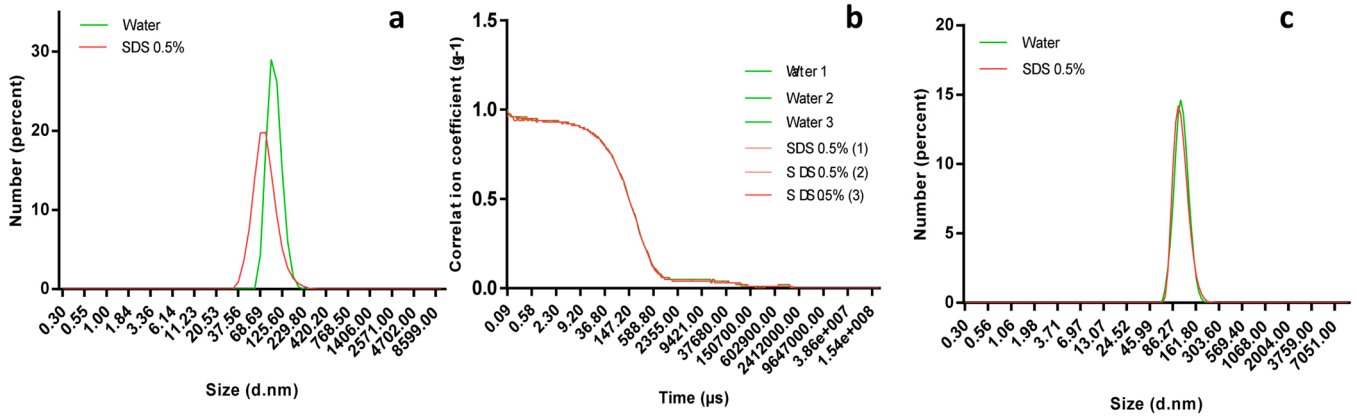

Fig. 5. Size distribution analysis by DLS. (a) Filtered and sonicated PET-NPLs samples were used with both water and SDS (0.5%) as dispersants, and 174.7 as the angle of scattering collection. (b) The correlation coefficients of the measurements. (c) Particle size distribution by using MADLS with three angles of scattering collection (174.7, 90, and 12.78) with water or SDS (0.5 %) as dispersants.

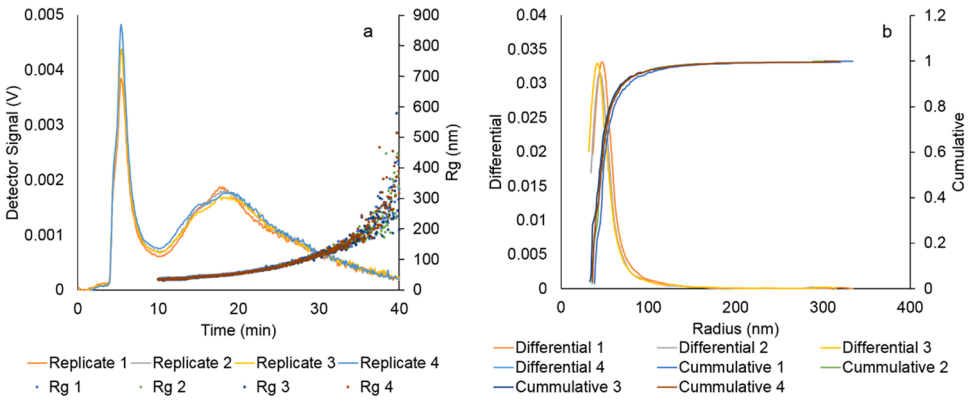

Fig. 6. AF4-MALS plots obtained for a 20 μL injection of 1 mg/mL of PET, (a) Fractogram (left axis: MALS 90° detector signal (V); right axis: Gyration Radius (Rg, nm)) and (b) Differential and Cumulative graphics.

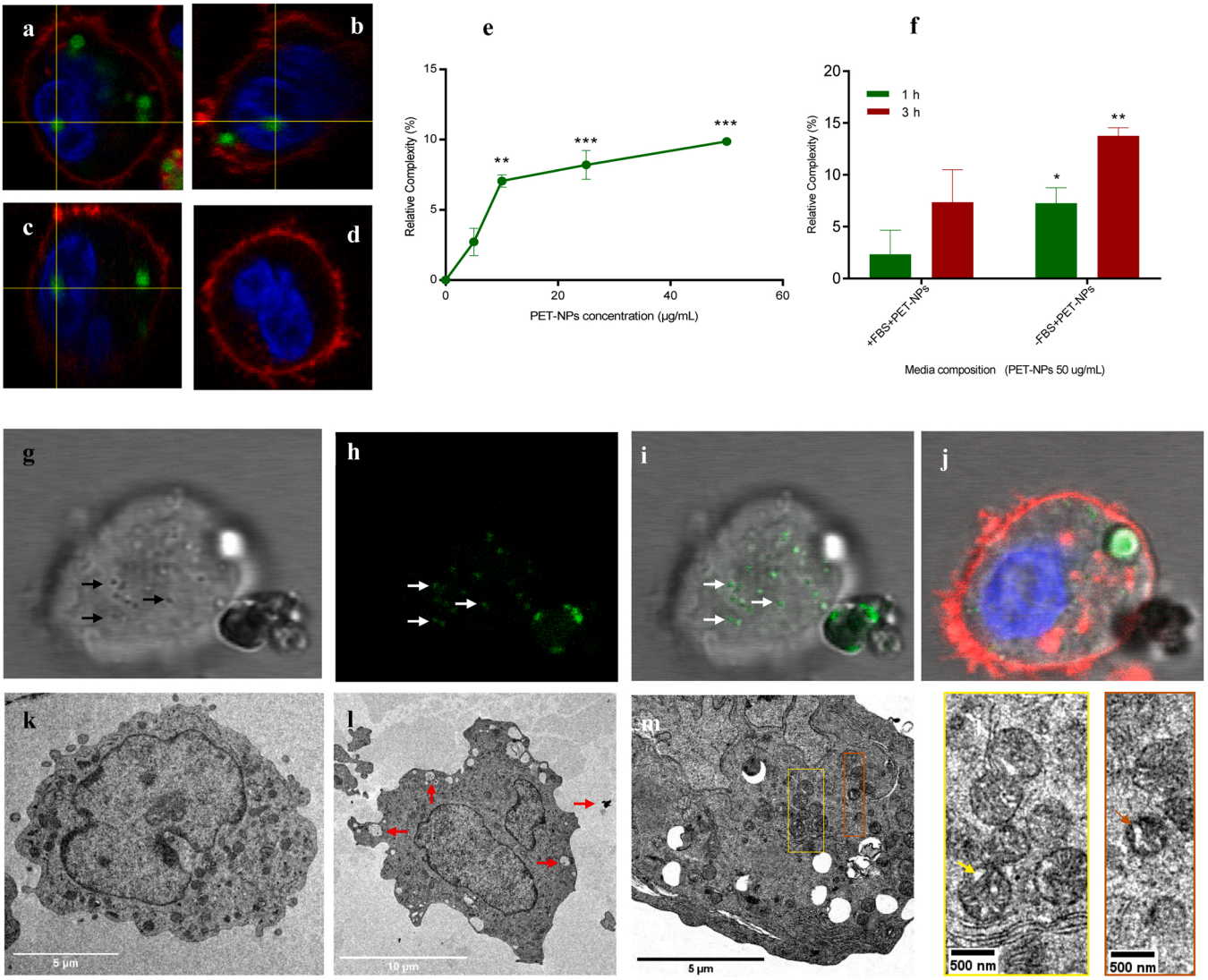

Fig. 7. Confocal orthogonal view of internalized Nile red stained PET-NPLs (green signal) on THP1 cells after 24 h exposure to 50 μg/mL is presented as XY, YZ and XZ (a, b and c respectively) three dimensional views and d is the control. Small dot like structures is observed at the cytoplasm of THP1 cells (g) and fluorescence at 546–628 on h is collected on the same points. Merged images are visualized on i where also the big fluorescent structure corresponds to fluorescent agglomerates. Relative increment on complexity at early exposition to 50 μg/mL of PET-NP on THP1 cells is represented on e (**$p < 0.018$, ***$p < 0.0009$ and ****$p < 0.0004$) and influence FBS on the media composition (f) (*$p < 0.0162$ and **$p < 0.0087$). For both cases One-way ANOVA with Dunnett's post-test was used for the statistical analysis. TEM images show an increment on vacuoles at 5 (l) or 50 (m) μg/mL of PET-NPs, relative to control (k), PET-NPs like structures are show by the red arrows and mitochondrial abnormalities or holey mitochondrion are present only on PET-NPs treated cells (yellow and brown arrows).

are significantly different in terms of complexity, with a higher uptake in the absence of serum.

3.2.3. Cell uptake detection by TEM

TEM has successfully been applied to detect nanomaterials uptake by many cell types, including MNPLs (Vila et al., 2017; Cortés et al., 2020). Our TEM figures show substantial amounts of PET-NPLs incorporated into cytoplasmic vesicles (Fig. 7l). Although no specific studies have been addressed to understand the cell uptake of PET-NPLs, their presence in the lysosomes of Caco-2 cells (Magrì et al., 2021) can suggest that their uptake is by endocytosis, as previously demonstrated for PS-NPLs where that was considered as the main cellular absorption pathway (Magrì et al., 2018; Cortés et al., 2020). Interestingly, we detect PETNPLs into mitochondria inducing some alterations. These effects have been also reported for PSNPLs (Cortés et al., 2020; Trevisan et al., 2020).

Taking all three approaches together, it seems clear that cells can uptake our lab-produced PET-NPLs.

3.3. Cytotoxicity

Cell viability curves were studied to determine the cytotoxic effects of PET-NPLs exposure on THP1 and TK6 cell-lines. As shown in Fig. 8 no significant cytotoxicity was observed up to the concentration of 100 μg/mL. Only mild effects were observed at the high concentration of 200 μg/mL of PET-NPLs on TK6, where the viability was compromised close to 80 % for exposures lasting for 48 h. Since our aim is to work with non-cytotoxic doses, the following experiments were carried out at concentrations up to 50 μg/mL.

This lack of toxicity of the obtained PET-NPLs agree with the reported for other secondary PET nanomaterials obtained using different methodological approaches (Magrì et al., 2018; Dhaka et al., 2022). Although the toxic effects of MNPLs can depend on distinctive characteristics, *i.e.*, the size, most of the studies agree with their lack of acute toxic effects. This has been proved when the effects of different MPLs (polyethylene, polypropylene, polyvinylchloride, and PET) were evaluated in three different cell lines (Stock et al., 2021). This means that other milder, sub-toxic cellular effects, and not cell death, must be selected as biomarker when evaluating the harmful effects associated with MNPLs exposure. Further efforts looking for different exposure scenarios, considering acute exposure to higher concentrations, repeated doses, or long-term exposures, are necessary to decipher the toxic effects of PET-NPLs obtained from environmental plastic samples.

3.4. ROS induction by PET-NPLs

The ability of our PET-NPLs to increase the intracellular levels of ROS was evaluated using the DHE detection assay, in THP1 cells. The results indicated in Fig. 9 show that exposures lasting for 3 h were unable to induce statistically significant differences in the ROS levels when compared to untreated controls. Nevertheless, the positive control used (antimycin) induced important levels of ROS, confirming the goodness of the used protocol. Although one of the most recognized mechanisms of action of nanomaterials is the induction of ROS (Karkossa et al., 2021), MNPLs seem to have a different behavior. Recent results with real PET samples did not show ROS induction in human intestinal Caco-2 cells (Magrì et al., 2021). This inability of PET-NPLs to induce oxidative stress *in vitro*, agree with many studies using PSNPLs as a model of MNPLs where exposure did not increase ROS levels in Caco-2 cells after acute exposures (Domenech et al., 2020) or after long-term exposures (Domenech et al., 2021). Nevertheless, the potential induction of oxidative stress seems to be dependent on the cell type as demonstrated with different hematopoietic cell lines where ROS was clearly observable (Rubio et al., 2020), as well as dependent on the particle size (Kik et al., 2021).

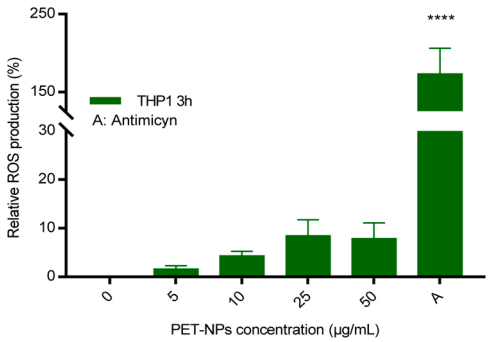

Fig. 9. Reactive oxygen species (ROS) induction in THP-1 cells after PET-NPLs exposures lasting for 3 h at concentrations ranging from 0 to 50 μg/mL at 3 h exposition. Data is expressed as percentage of ROS production relative to the untreated control ± SEM. One-way ANOVA with Dunnett's post-test was performed. Statistical significance indicated on the graph as ****$p < 0.0001$.

3.5. Genotoxic evaluation of PET-NPLs by using the comet assay

Among the different biomarkers evaluating health risk, those detecting genotoxicity stand out. This is because, due to the main role of DNA in cell functionality, DNA damage severely compromises human health (Carbone et al., 2020). Although the genotoxicity assays can evaluate both primary or fixed DNA damage, those detecting primary damage are much more sensitive. Thus, the comet assay is used to measures the induction of single/double DNA breaks as well as the induction of oxidative damage on the DNA bases. Its simplicity and sensitivity have spread its use in many fields, including the hazard assessment of nanomaterials (García-Rodríguez et al., 2019).

In our study, we have not been able to demonstrate the ability of our PET-NPLs to damage DNA, as indicated in Fig. 10. In addition to the lack of direct strand breaks (Fig. 10a) PET-NPLs exposure also did not induce oxidative damage on the DNA bases (Fig. 10b). These results agree with

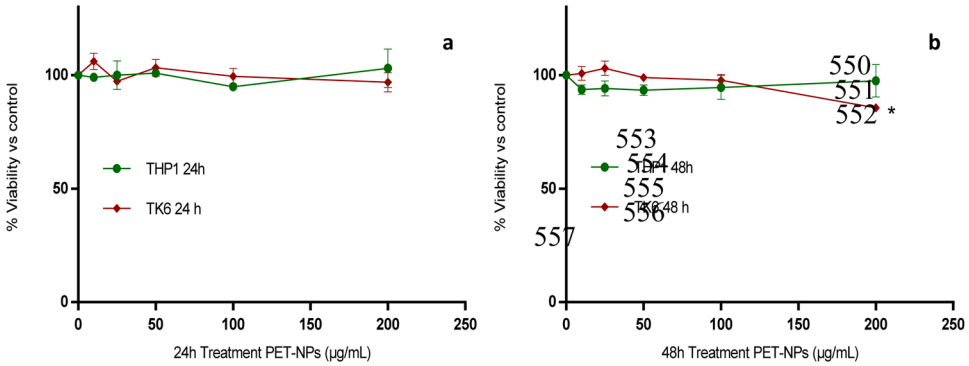

Fig. 8. Relative cell viability of THP1 (green) and TK6 (red) cell lines at concentrations ranging from 0 to 200 μg/mL, after PET-NPLs exposures lasting for 24 h (a) and 48 h (b). Data represented as percentage of living cells relative to the untreated control treatment at 24 (green) and 48 (blue) h of exposure. Data is expressed as percentage of cells relative to the untreated control ± SEM. One-way ANOVA with Dunnett's post-test was used for the statistical analysis. Statistical significance indicated on the graph as * $p < 0.01$.

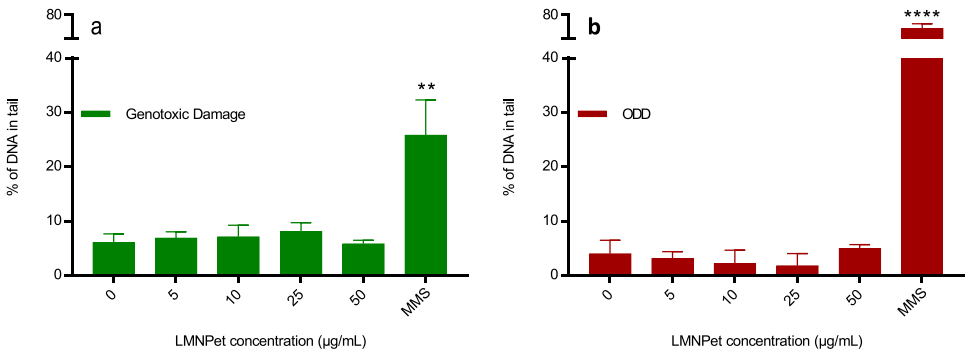

Fig. 10. THP1 genotoxic (a) and oxidative DNA damage (b) at concentrations ranging from 0 to 50 µg/mL and exposure lasting for 3 h. Damage is expressed as the percentage DNA in tail ± SEM. One-way ANOVA with Dunnett's post-test was performed. Statistical significance indicated on the graph as $^{**}P < 0.01$ ****p < 0.0001. respectively. Methyl methanesulfonate (MMS) was used as a positive control.

our previous data showing that PET-NPLs were unable to induce oxidative stress. No other studies are using PET where the genotoxic potential was evaluated. Nevertheless, a few studies on the genotoxic potential of polystyrene MNPLs have been reported showing contradictory results. In *in vitro* studies, negative findings using the micronucleus assay were observed in the intestinal/placenta barrier cells exposed to 50/500 nm polystyrene NPLs (Hesler et al., 2020). Negative results were also reported in human intestinal Caco-2 cells exposed to 50 nm polystyrene NPLs both as a component of an *in vitro* barrier (Domenech et al., 2020) or after long-term exposures (Domenech et al., 2021). Nevertheless, positive effects were observed in sh27 fibroblasts using the micronucleus assay (Poma et al., 2019). This would indicate differences between cell types in both MNPLs uptake and genotoxic effects as reported when different types of human hematopoietic cell lines were used (Rubio et al., 2020).

As a summing up, we consider that the proposed method to obtain uniform and reproducible secondary NPLs from representative environmental plastic goods is adequate, since the nano sized fraction of the suspension is very high (about 95%). In addition, we consider that the obtained samples mimic the naturally occurring degradation phenomenon The characterization of the working material by TEM showed a bimodal distribution in the nano range with most of the particles ranging around 50 nm. Simple filtering and sonication steps produce a uniform distribution around 100 nm when DLS and AF4 measurements are applied. We are confident that this methodology can be easily used to obtain NPLs from other plastics materials, scaping from the constrictions posed using pristine forms of commercial polystyrene NPLs. Materials resulting from environmentally representative plastics permit to answer the main open questions asking for the risks of environmental MNPLs resulting from degradation processes. As reported, our protocol using non-metallic burrs during the sanding process has a great advantage over those using metallic blades which contaminate the resulting MNPLs. Such metallic contamination would invalidate any approach aiming to evaluate the potential health risk of such types of MNPLs. It must be recalled that most of the studies evaluating the hazardous effects of MNPLs use sizes in the micro range. Although they can provide useful information, it must be remembered that plastic particles sized in the nano-range are more prone to cross epithelial barriers and, consequently, spread over the different tissues and organs. Accordingly, to be able to get nanoplastics -instead of microplastics- resulting from the degradation of representative environmental plastic pollutants can represent an important step to get more sound data answering about their potential effects on human health.

Although our hazard approach can be considered just as a preliminary one, it is important to highlight that the obtained PET-NPLs are easily internalized by the used cell models without important toxic or genotoxic effects. Due to the lack of *gross* biological effects, reported by many authors using different sized MNPLs, the use of methodological approaches detecting other types of milder cell effects, out of cell death, should be used when evaluating the harmful effects associated with MNPLs exposure (Stock et al., 2021). In such a context, having the facility of easily obtaining different types of MNPLs can result very helpful. It is obvious that the original sources of the environmental commercial PET plastics can differ in factors such as crystallinity and plasticizer content. This can suppose differences in the obtained samples, hence differences in their induced biological effects. However, this should not necessarily be considered a problem but rather a challenge, since the obtained/evaluated samples are more representative of the environmentally MNPLs pollutants.

CRediT authorship contribution statement

RM and AH planned the experiments. AV, LR, MA, MLM, VFC, and OHM carried out the experimental part. AV analyzed the data, carried out the statistical analysis, and prepared tables/figures. AV, RM, and AH wrote the final manuscript.

Declaration of Competing Interest

The authors declare that they have no known competing financial interests or personal relationships that could have appeared to influence the work reported in this paper.

Data availability

Data will be made available on request.

Acknowledgments

A. Villacorta was supported by Ph.D. fellowships from the National Agency for Research and Development (ANID), CONICYT PFCHA / DOCTORADO BECAS CHILE / 2020 – 72210237. L. Rubio was supported by the Fondo Nacional de Innovación y Desarrollo Científico y Tecnológico (FONDOCYT) República Dominicana (Project 2018–2019-2B2–093). This project (PlasticHeal) has received funding from the European Union's Horizon 2020 research and innovation program under grant agreement No 965196. L. Rubio was supported by a contract Juan de la Cierva (IJC2020-2686I/AEI/10.13039/501100011033).

Environmental Implication

In spite of the intrinsic interest in understanding the potential hazards associated with the environmental micro-/nanoplastics exposure, most of the studies use pristine commercial samples. Thus, a challenge is to get/evaluate environmental representative samples. In this context, we propose a method to obtain *real* environmental samples of

nanoplastics. Initially applied to PET water bottles, the proposed method is applicable to any source of environmental plastic goods. Interestingly, during the improvement of the method, we discover potential metal contamination resulting from other proposed milling procedures. Our method avoids such contamination, which benefits the ulterior hazard evaluations.

Appendix A. Supporting information

Supplementary data associated with this article can be found in the online version at doi:10.1016/j.jhazmat.2022.129593.

References

Ali, M.U., Lin, S., Yousaf, B., Abbas, Q., Munir, M.A.M., Ali, M.U., Rasihd, A., Zheng, C., Kuang, X., Wong, M.H., 2021b. Environmental emission, fate and transformation of microplastics in biotic and abiotic compartments: global status, recent advances and future perspectives. Sci. Total Environ. 791, 148422 https://doi.org/10.1016/j.scitotenv.2021.148422.

Ali, S.S., Elsamahy, T., Koutra, E., Kornaros, M., El-Sheekh, M., Abdelkarim, E.A., Zhu, D., Sun, J., 2021a. Degradation of conventional plastic wastes in the environment: a review on current status of knowledge and future perspectives of disposal. Sci. Total Environ. 771, 144719 https://doi.org/10.1016/j.scitotenv.2020.144719.

Andanson, J.M., Kazarian, S.G., 2008. In situ ATR-FTIR spectroscopy of poly(ethylene terephthalate) subjected to high-temperature temthanol. Macromol. Symp. 265, 195–204. https://doi.org/10.1002/masy.200850521.

Astner, A.F., Hayes, D.G., O'Neill, H., Evans, B.R., Pingali, S.V., Urban, V.S., Young, T.M., 2019. Mechanical formation of micro- and nano-plastic materials for environmental studies in agricultural ecosystems. Sci. Total Environ. 685, 1097–1106. https://doi.org/10.1016/j.scitotenv.2019.06.241.

Balakrishnan, G., Déniel, M., Nicolai, T., Chassenieux, C., Lagarde, F., 2019. Towards more realistic reference microplastics and nanoplastics: preparation of polyethylene micro/nanoparticles with a biosurfactant. Environ. Sci. Nano 6, 315–324. https://doi.org/10.1039/C8EN01005F.

Ballesteros, S., Domenech, J., Barguilla, I., Cortés, C., Marcos, R., Hernández, A., 2020. Genotoxic and immunomodulatory effects in human white blood cells after *ex vivo* exposure to polystyrene nanoplastics. Environ. Sci. Nano 7, 3431–3446. https://doi.org/10.1039/D0EN00748J.

Batool, I., Qadir, A., Levermore, J.M., Kelly, F.J., 2021. Dynamics of airborne microplastics, appraisal and distributional behaviour in atmosphere; a review. Sci. Total Environ. 14, 150745 https://doi.org/10.1016/j.scitotenv.2021.150745.

Borrelle, S.B., Ringma, J., Law, K.L., Monnahan, C.C., Lebreton, L., McGivern, A., Murphy, E., Jambeck, J., Leonard, G.H., Hilleary, M.A., Eriksen, M., Possingham, H. P., De Frond, H., Gerber, L.R., Polidoro, B., Tahir, A., Bernard, M., Mallos, N., Barnes, M., Rochman, C.M., 2020. Predicted growth in plastic waste exceeds efforts to mitigate plastic pollution. Science 369, 1515–1518. https://doi.org/10.1126/science.aba3656.

Carbone M, Arron ST, Beutler B, Bononi A, Cavenee W, Cleaver JE, Croce CM, D'Andrea A, Foulkes WD, Gaudino G, Groden JL, Henske EP, Hickson ID, Hwang PM, Kolodner RD, Mak TW, Malkin D, Monnat RJ Jr, Novelli F, Pass HI, Petrini JH, Schmidt LS, Yang H. Tumour predisposition and cancer syndromes as models to study gene-environment interactions. Nat Rev Cancer, 2020, 20(9): 533-549. doi: 10.1038/s41568-020-0265-y.

Chen, Z., Hay, J.N., Jenkins, M.J., 2013. The thermal analysis of poly(ethylene terephthalate) by FTIR spectroscopy. Thermochim. Acta 552, 123–130. https://doi.org/10.1016/j.tca.2012.11.002.

Cortés, C., Domenech, J., Salazar, M., Pastor, S., Marcos, R., Hernández, A., 2020. Nanoplastics as a potential environmental health factor: effects of polystyrene nanoparticles on human intestinal epithelial Caco-2 cells. Environ. Sci. Nano 7, 272–285. https://doi.org/10.1039/C9EN00523D.

Dhaka, V., Singh, S., Anil, A.G., Sunil Kumar Naik, T.S., Garg, S., Samuel, J., Kumar, M., Ramamurthy, P.C., Singh, J., 2022. Occurrence, toxicity and remediation of polyethylene terephthalate plastics. A review. J. Environ. Chem. Lett. 13, 1–24. https://doi.org/10.1007/s10311-021-01384-8.

Domenech, J., Hernández, A., Rubio, L., Marcos, R., Cortés, C., 2020. Interactions of polystyrene nanoplastics with *in vitro* models of the intestinal barrier. Arch. Toxicol. 94 (9), 2997–3012. https://doi.org/10.1007/s00204-020-02805-3.

Domenech, J., de Britto, M., Velázquez, A., Pastor, S., Hernández, A., Marcos, R., Cortés, C., 2021. Long-term effects of polystyrene nanoplastics in human intestinal Caco-2 cells. Biomolecules 11, 1442. https://doi.org/10.3390/biom11101442.

ECHA, (2018) European Chemicals Agency. Background document on the Opinion on the Annex XV report proposing restrictions on intentionally added microplastics. ⟨https://echa.europa.eu/documents/10162/2ddaab18–76d6–49a2-ec46–8350dabf5dc⟩.

Evangeliou, N., Grythe, H., Klimont, Z., Heyes, C., Eckhardt, S., Lopez-Aparicio, S., Stohl, A., 2020. Atmospheric transport is a major pathway of microplastics to remote regions. Nat. Commun. 11 (1), 3381. https://doi.org/10.1038/s41467-020-17201-9.

García-Rodríguez, A., Rubio, L., Vila, L., Xamena, N., Velázquez, A., Marcos, R., Hernández, A., 2019. The comet assay as a tool to detect the genotoxic potential of nanomaterials. Nanomaterials 9, 1385. https://doi.org/10.3390/nano9101385.

Gwada, B., Ogendi, G., Makindi, S.M., Trott, S., 2019. Composition of plastic waste discarded by households and its management approaches. Glob. J. Environ. Sci. Manag. 5, 83–94. https://doi.org/10.22034/gjesm.2019.01.07.

Hartmann, N.B., Hüffer, T., Thompson, R.C., Hassellöv, M., Verschoor, A., Daugaard, A. E., Rist, S., Karlsson, T., Brennholt, N., Cole, M., Herrling, M.P., Hess, M.C., Ivleva, N. P., Lusher, A.L., Wagner, M., 2019. Are we speaking the same language? Recommendations for a definition and categorization framework for plastic debris. Environ. Sci. Technol. 53 (3), 1039–1047. https://doi.org/10.1021/acs.est.8b05297.

Hesler M, Aengenheister L, Ellinger B, Drexel R, Straskraba S, Jost C, Wagner S, Meier F, von Briesen H, Büchel C, Wick P, Buerki-Thurnherr T, Kohl Y. Multi-endpoint toxicological assessment of polystyrene nano- and microparticles in different biological models in vitro. Toxicol In Vitro, 2019, 61: 104610. doi: 10.1016/j.tiv.2019.104610.

Johnson, L.M., Mecham, J.B., Krovi, S.A., Moreno Caffaro, M.M., Aravamudhan, S., Kovach, A.L., Fennell, T.R., Mortensen, N.P., 2021. Fabrication of polyethylene terephthalate (PET) nanoparticles with fluorescent tracers for studies in mammalian cells. Nanoscale Adv. 3, 339–346. https://doi.org/10.1039/D0NA00888E.

Karkossa, I., Bannuscher, A., Hellack, B., Wohlleben, W., Laloy, J., Stan, M.S., Dinischiotu, A., Wiemann, M., Luch, A., Haase, A., von Bergen, M., Schubert, K., 2021. Nanomaterials induce different levels of oxidative stress, depending on the used model system: comparison of *in vitro* and *in vivo* effects. Sci. Total Environ. 801, 149538 https://doi.org/10.1016/j.scitotenv.2021.149538.

Kik, K., Bukowska, B., Krokosz, A., Sicińska, P., 2021. Oxidative properties of polystyrene nanoparticles with different diameters in human peripheral blood mononuclear cells (*In vitro* study). Int J. Mol. Sci. 22 (9), 4406. https://doi.org/10.3390/ijms22094406.

Lionetto, F., Corcione, C.E., Rizzo, A., Maffezzoli, A., 2021. Production and characterization of polyethylene terephthalate nanoparticles. Polymers 13 (21), 3745. https://doi.org/10.3390/polym13213745.

Lohrke, J., Briel, A., Mäder, K., 2008. Characterization of superparamagnetic iron oxide nanoparticles by asymmetrical flow-field-flow-fractionation. Nanomedicine 3 (4), 437–452. https://doi.org/10.2217/17435889.3.4.437.

Magrì, D., Veronesi, M., Sánchez-Moreno, P., Tolardo, V., Bandiera, T., Pompa, P.P., Athanassiou, A., Fragouli, D., 2021. PET nanoplastics interactions with water contaminants and their impact on human cells. Environ. Pollut. 271, 116262 https://doi.org/10.1016/j.envpol.2020.116262.

Magrì, D., Sánchez-Moreno, P., Caputo, G., Gatto, F., Veronesi, M., Bardi, G., Catelani, T., Guarnieri, D., Athanassiou, A., Pompa, P.P., Fragouli, D., 2018. Laser ablation as a versatile tool to mimic polyethylene terephthalate nanoplastic pollutants: characterization and toxicology assessment. ACS Nano 12 (8), 7690–7700. https://doi.org/10.1021/acsnano.8b01331.

Nanogenotox protocol. Final protocol for producing suitable manufactured nanomaterial exposure media. Nanogenotox, towards a method for detecting the potential genotoxicity of nanomaterials, 2011. ⟨https://www.anses.fr/en/system/files/nanogenotox_deliverable_5.pdf⟩. Accessed on 15/01/2022.

Parolini, M., Ferrario, C., De Felice, B., Gazzotti, S., Bonasoro, F., Candia Carnevali, M.D., Ortenzi, M.A., Sugni, M., 2020. Interactive effects between sinking polyethylene terephthalate (PET) microplastics deriving from water bottles and a benthic grazer. J. Hazard. Mater. 398, 122848 https://doi.org/10.1016/j.jhazmat.2020.122848.

Pignattelli, S., Broccoli, A., Piccardo, M., Felline, S., Terlizzi, A., Renzi, M., 2021. Short-term physiological and biometrical responses of *Lepidium sativum* seedlings exposed to PET-made microplastics and acid rain. Ecotoxicol. Environ. Saf. 208, 111718 https://doi.org/10.1016/j.ecoenv.2020.111718.

PlasticsEurope, – The Facts 2018**:** An analysis of european plastics production, demand and waste data. ⟨https://plasticseurope.org/wp-content/uploads/2021/10/2018-Plastics-the-facts.pdf⟩.

Prata, J.C., Reis, V., Matos, J.T.V., da Costa, J.P., Duarte, A.C., Rocha-Santos, T., 2019. A new approach for routine quantification of microplastics using Nile Red and automated software (MP-VAT. Sci. Total Environ. 690, 1277–1283. https://doi.org/10.1016/j.scitotenv.2019.07.060.

Rai, P.K., Lee, J., Brown, R.J.C., Kim, K.H., 2021. Environmental fate, ecotoxicity biomarkers, and potential health effects of micro- and nano-scale plastic contamination. J. Hazard. Mater. 403, 123910 https://doi.org/10.1016/j.jhazmat.2020.123910.

Rodríguez-Hernández, A.G., Muñoz-Tabares, J.A., Aguilar-Guzmán, J.C., Vazquez-Duhalt, R., 2019. A novel and simple method for polyethylene terephthalate (PET) nanoparticle production. Environ. Sci. Nano 6 (7), 2031–2036. https://doi.org/10.1039/c9en00365g.

Rubio, L., Annangi, B., Vila, L., Hernández, A., Marcos, R., 2016. Antioxidant and anti-genotoxic properties of cerium oxide nanoparticles in a pulmonary-like cell system. Arch. Toxicol. 90, 269–278. https://doi.org/10.1007/s00204-015-1468-y.

Rubio, L., Barguilla, I., Domenech, J., Marcos, R., Hernández, A., 2020. Biological effects, including oxidative stress and genotoxic damage, of polystyrene nanoparticles in different human hematopoietic cell lines. J. Hazard. Mater. 398, 122900 https://doi.org/10.1016/j.jhazmat.2020.122900.

Shruti, V.C., Pérez-Guevara, F., Roy, P.D., Kutralam-Muniasamy, G., 2022. Analyzing microplastics with Nile Red: emerging trends, challenges, and prospects. J. Hazard. Mater. 423 (Pt B), 127171 https://doi.org/10.1016/j.jhazmat.2021.127171.

Stock, V., Laurisch, C., Franke, J., Dönmez, M.H., Voss, L., Böhmert, L., Braeuning, A., Sieg, H., 2021. Uptake and cellular effects of PE, PP, PET and PVC microplastic particles. Toxicol. Vitr. 70, 105021 https://doi.org/10.1016/j.tiv.2020.105021.

Trevisan, R., Uzochukwu, D., Di Giulio, R.T., 2020. PAH sorption to nanoplastics and the Trojan horse effect as drivers of mitochondrial toxicity and PAH localization in zebrafish. Front. Environ. Sci. 8, 78. https://doi.org/10.3389/fenvs.2020.00078.

Turner, A., Filella, M., 2021. Hazardous metal additives in plastics and their environmental impacts. Environ. Int. 156, 106622 https://doi.org/10.1016/j.envint.2021.106622.

Vila, L., Rubio, L., Annangi, B., García-Rodríguez, A., Marcos, R., Hernández, A., 2017. Frozen dispersions of nanomaterials are a useful operational procedure in nanotoxicology. Nanotoxicology 11, 31–40. https://doi.org/10.1080/17435390.2016.1262918.

Zitouni, N., Bousserrhine, N., Missawi, O., Boughattas, I., Chèvre, N., Santos, R., Belbekhouche, S., Alphonse, V., Tisserand, F., Balmassiere, L., Dos Santos, S.P., Mokni, M., Guerbej, H., Banni, M., 2021. Uptake, tissue distribution and toxicological effects of environmental microplastics in early juvenile fish *Dicentrarchus labrax*. J. Hazard. Mater. 403, 124055 https://doi.org/10.1016/j.jhazmat.2020.124055.